

Investigation of the scale dependence in the MSR and $\overline{\text{MS}}$ top quark mass schemes for the $t\bar{t}$ invariant mass differential cross section using LHC data

Toni Mäkelä^{*a,b}, André H. Hoang^{†c,d}, Katerina Lipka^{‡a,e}, and Sven-Olaf Moch^{§f}

^aDeutsches Elektronen-Synchrotron, Notkestr. 85, 22607 Hamburg, Germany

^bNational Centre for Nuclear Research, Pasteura 7, PL-02-093 Warsaw, Poland

^cFaculty of Physics, University of Vienna, Boltzmanngasse 5, A-1090 Vienna, Austria

^dErwin Schrödinger Institute for Mathematics and Physics, University of Vienna, Boltzmanngasse 9, A-1090 Vienna, Austria

^eFakultät für Mathematik und Naturwissenschaften, Bergische Universität Wuppertal, Gaußstrasse 20, D-42119 Wuppertal, Germany

^fII. Institut für Theoretische Physik, Universität Hamburg, Luruper Chaussee 149, D-22761 Hamburg, Germany

September 8, 2023

Abstract

The computation of the single-differential top quark-antiquark pair ($t\bar{t}$) production cross section at NLO in the fixed-order expansion is examined consistently using the MSR and $\overline{\text{MS}}$ short-distance top quark mass schemes. A thorough investigation of the dependence of different regions of the $t\bar{t}$ invariant mass spectrum on the renormalization scales R and μ_m of the MSR mass $m_t^{\text{MSR}}(R)$ and $\overline{\text{MS}}$ mass $\overline{m}_t(\mu_m)$, respectively, is carried out. We demonstrate that a scale choice of $R \sim 80$ GeV is important for the stability of the cross-section predictions for the low $t\bar{t}$ invariant mass range, which is important for a reliable extraction of the top quark mass. Furthermore, a choice of semi-dynamical renormalization and factorization scales is preferred. These findings are expected to remain valid once non-relativistic quasi-bound state effects are included in the low invariant mass region.

*toni.makela@cern.ch

†andre.hoang@univie.ac.at

‡katerina.lipka@desy.de

§sven-olaf.moch@desy.de

1 Introduction

The top quark mass m_t is a fundamental parameter of the Standard Model and has an important role in many predictions, both directly and via higher-order corrections. For instance, together with the values of the strong coupling constant α_s and the mass of the Higgs boson, it determines the stability of the electroweak vacuum [1–4]. Yet, quark masses are formal parameters of the Standard Model QCD Lagrangian and depend on the adopted renormalization scheme. The frequently used top quark pole mass m_t^{pole} is based on the concept of an on-shell observable particle and entails that real and virtual self-energy radiation can be resolved at arbitrarily small energy scales. While the picture of an on-shell top quark allows for consistent cross section field theory computations, it is not physical because the top quark is a colored object and decays. This results in a sizeable linear infrared (IR) sensitivity of m_t^{pole} of the order of the QCD scale Λ_{QCD} [5–7]¹ which leads to the pole mass renormalon problem at high orders in perturbation theory. Quark masses defined in so-called short-distance mass schemes such as the modified minimal subtraction ($\overline{\text{MS}}$) scheme [10, 11] mass $\overline{m}_t(\mu_m)$, or the MSR scheme [12, 13] mass $m_t^{\text{MSR}}(R)$, do not have this issue, and their renormalization scales μ_m and R , respectively, act as a finite resolution scale. This means that real and virtual self-energy radiation are treated inclusively for the scales below μ_m and R . The absence of the $\mathcal{O}(\Lambda_{\text{QCD}})$ renormalon problem, together with the additional freedom to adopt suitable choices for μ_m and R , can be very useful to achieve higher precision concerning the m_t dependence in top mass sensitive observables. In particular, the freedom of scheme and scale choice is important for predictions at lower orders, since it leads to a systematic absorption of sizeable corrections, not originating from the pole mass renormalon, into the quark mass parameter.

A well-known example is the highly m_t -sensitive $t\bar{t}$ cross section at the production threshold in e^+e^- annihilation, where switching from the pole mass scheme to the threshold mass schemes such as the PS (at the scale of around 25 GeV) or the 1S mass schemes can minimize the large $t\bar{t}$ quasi-bound state corrections at any order, since these mass schemes encode a sizeable fraction of the binding energy corrections $\Delta E \sim m_t \alpha_s^2$ into the mass value [14]. In the case of the $t\bar{t}$ quasi-bound state, the scale choice for the PS mass is related to the fact that these m_t -sensitive bound state corrections arise from physical dynamical scales of the order of the inverse Bohr radius $\langle 1/r_B \rangle \sim m_t \alpha_s \sim 25$ GeV, and the MSR mass $m_t^{\text{MSR}}(25 \text{ GeV})$ is a suitable choice as well [13]. Thus, the scale dependence of $\overline{m}_t(\mu_m)$ and $m_t^{\text{MSR}}(R)$ allows to properly adapt to these dynamical scales of the top mass sensitivity for an observable under consideration. The respective renormalization group equations (RGEs) and matching relations provide the tool to unambiguously relate the m_t values extracted at different dynamical scales. This concept is well known for the running strong coupling α_s and applies to the quark masses as well.

In this work, the dependence of the invariant mass of the $t\bar{t}$ pair, $m_{t\bar{t}}$, on the MSR mass scale

¹We note that linear IR sensitivities arise in cross sections whenever cuts on soft radiation are imposed, see e.g. Ref. [8]. These are associated to physical nonperturbative corrections in contrast to the pole mass, where the IR sensitivity arises purely from the choice of scheme [9].

R and the $\overline{\text{MS}}$ mass scale μ_m is investigated concurrently, for the first time, accounting for QCD corrections. Using experimental measurements of $t\bar{t}$ production at the LHC at $\sqrt{s} = 13 \text{ TeV}$ [15], the next-to-leading order (NLO) prediction of the $m_{t\bar{t}}$ differential cross section from Refs. [16, 17] and the scheme implementation procedure of Refs. [18, 19], we demonstrate that the proper scheme choice – which concerns the proper kind of top mass scheme *and* the renormalization scale – is of key importance and affects the size of higher-order corrections as well as the resulting value of the extracted top quark mass. Our analysis provides in particular a re-investigation of the “indirect” m_t^{pole} measurement of Ref. [20] by the CMS Collaboration which obtained $m_t^{\text{pole}} = 170.5 \pm 0.8 \text{ GeV}$ based on the same NLO theory prediction. This result is systematically lower than other indirect pole mass measurements [21–23] and was reconfirmed by the subsequent analysis in Ref. [24]. The latter analysis also extracted the MSR mass at the low scale $R = 3 \text{ GeV}$, $m_t^{\text{MSR}}(R = 3 \text{ GeV})$, yielding a low value as well, consistent with Ref. [20] after conversion to a common reference scheme. In the present analysis, we show that using the MSR mass $m_t^{\text{MSR}}(R = 80 \text{ GeV})$ would lead to a larger value, compatible with earlier measurements, after conversion to a common reference scheme. We provide general arguments that this particular scale choice leads to a systematic resummation of sizeable higher order QCD corrections that arise in the $t\bar{t}$ threshold region at the LHC, where the $t\bar{t}$ pairs are produced in color singlet as well as octet states and sizeable bins of the $m_{t\bar{t}}$ distribution are used in the analysis. This summation does not take place either in the pole mass scheme or when $m_t^{\text{MSR}}(R = 3 \text{ GeV})$ is used, explaining the results obtained in Refs. [20, 24]. The result of our investigation constitutes an important recommendation relevant for upcoming top quark mass measurements from differential $t\bar{t}$ production cross sections at the LHC. We note that the theoretical prediction used in the present analysis does not account for the next-to-next-to-leading order (NNLO) corrections [25, 26] or resummed Coulomb-type quasi-bound state corrections [27–29]. A coherent theory code that accounts for these results in a way adequate for the needs of the presented analysis is not yet available in either mass scheme. We also note that recently the MSR mass has been investigated by the ATLAS collaboration in Ref. [30] in the context of simulation and top mass calibration studies of the groomed jet mass for boosted top production.

In Sec. 2, we review the $\overline{\text{MS}}$ and MSR top quark mass schemes and the formulae to implement them, and in Sec. 3 we carry out a detailed investigation concerning the best choice of the MSR renormalization scale R . In Sec. 4 we quote the results for $m_t^{\text{MSR}}(R = 1 \text{ GeV})$ and higher R values from the fits to the LHC measurements, demonstrating the impact of the renormalization scale choice. We close in Sec. 5 with a summary and an outlook on future improvements.

2 Running m_t and the $t\bar{t}$ pair production cross section at NLO

In terms of a general mass renormalization scale μ_m , the pole and $\overline{\text{MS}}$ masses are related in perturbative QCD as

$$m_t^{\text{pole}} = \overline{m}_t(\mu_m) \left(1 + \sum_{n=1} d_n^{\overline{\text{MS}}}(\mu_m) \left(a_s^{(6)}(\mu_m) \right)^n \right), \quad (2.1)$$

where $a_s \equiv \alpha_s/\pi$. Here and everywhere else in this study, we explicitly indicate by the superscript whether we use the strong coupling $\alpha_s^{(5)}$ in the 5-flavor or $\alpha_s^{(6)}$ in the 6-flavor scheme. For the parton distribution functions (PDFs) only the 5-flavor scheme is employed. All quarks except for the top quark are treated as massless. The coefficients $d_n^{\overline{\text{MS}}}(\mu_m)$ in Eq. (2.1) are known up to four loops [31] and the first few orders read [32–34]

$$\begin{aligned} d_1^{\overline{\text{MS}}}(\mu_m) &= 4/3 + L, \\ d_2^{\overline{\text{MS}}}(\mu_m) &= 7.1952 + 4.6806L + 1.4167L^2, \\ d_3^{\overline{\text{MS}}}(\mu_m) &= 54.161 + 21.776L + 9.2026L^2 + 1.7940L^3, \end{aligned} \quad (2.2)$$

where the expansion uses $\alpha_s^{(6)}$ in the 6-flavor scheme and $L = \log((\mu_m/\overline{m}(\mu_m))^2)$. The running of the $\overline{\text{MS}}$ mass is described by the RGE

$$\mu_m^2 \frac{d\overline{m}_t(\mu_m)}{d\mu_m^2} = -\overline{m}_t(\mu_m) \sum_{i=0} \gamma_i^m \left(a_s^{(6)}(\mu) \right)^{i+1}, \quad (2.3)$$

where the anomalous dimensions γ_i^m are known to five loops [35, 36]. The first few orders [37–42] are given by

$$\begin{aligned} \gamma_0^m &= 1, \\ \gamma_1^m &= 3.3750, \\ \gamma_2^m &= 4.8387, \\ \gamma_3^m &= -4.5082. \end{aligned} \quad (2.4)$$

Electroweak corrections (see, e.g. [43, 44]) are not considered. The RGE in Eq. (2.3) has the solution

$$\overline{m}_t(\mu_1) = \overline{m}_t(\mu_0) \exp \left\{ -2 \sum_{i=0} \int_{\mu_0}^{\mu_1} \frac{d\mu}{\mu} \gamma_i^m \left(a_s^{(6)}(\mu) \right)^{i+1} \right\}, \quad (2.5)$$

yielding the $\overline{\text{MS}}$ mass at a scale μ_1 via evolution from the known mass at a reference scale μ_0 . Here and below we quote relations at $\mathcal{O}(\alpha_s^3)$ and evolution equations at $\mathcal{O}(\alpha_s^4)$. We have also used these relations in our analysis for determining numerical values for the quark masses (and the strong coupling), even though our cross section analysis is based on a fixed-order theory description at NLO. Since the mass (and strong coupling) matching relations and RGE equations are well convergent series and no subtle cancellations between the different ingredients need to be taken care of (which would be the case for the PDFs) this approach is fully consistent and has the advantage that the theoretical uncertainties in the numerical values of the masses (and the strong coupling) are eliminated entirely from our analysis. We recommend this approach also for future phenomenological analyses. For implementing different mass schemes in the analytic expression for the differential $m_{t\bar{t}}$ cross sections at NLO, see Eq. (2.14) below, only the $\mathcal{O}(\alpha_s)$ coefficients from Eqs. (2.1) and (2.6) are used.

The $\overline{\text{MS}}$ mass is by construction a 6-flavor quantity and should only be used in observables where the dynamical scale of the top-quark mass sensitivity is of order m_t or larger, i.e. $\mu_m \gtrsim m_t$. The MSR mass is, like the $\overline{\text{MS}}$ mass, determined from top-quark self-energy corrections [13, 45], but designed such that all virtual and off-shell top-quark quantum fluctuations are integrated out in the on-shell limit.² The MSR mass $m_t^{\text{MSR}}(R)$ is therefore a 5-flavor quantity and its R -dependence properly captures all radiation off the top quark that is soft in the top quark rest frame, which is not the case for the $\overline{\text{MS}}$ mass. The MSR mass is the proper choice if the dynamical scale of the top quark mass sensitivity is below m_t , i.e. $R \lesssim m_t$.

The pole and MSR masses are related as

$$m_t^{\text{pole}} = m_t^{\text{MSR}}(R) + R \sum_{n=1}^{\infty} d_n^{\text{MSR}} \left(a_s^{(5)}(R) \right)^n, \quad (2.6)$$

where the coefficients d_n^{MSR} read [13]

$$\begin{aligned} d_1^{\text{MSR}} &= 4/3, \\ d_2^{\text{MSR}} &= 8.1330 \\ d_3^{\text{MSR}} &= 71.602. \end{aligned} \quad (2.7)$$

In the limit $R \rightarrow \overline{m}_t(\overline{m}_t)$, $m_t^{\text{MSR}}(R)$ approaches the $\overline{\text{MS}}$ mass $\overline{m}_t(\overline{m}_t)$ and matches on it in analogy to the 5-flavor and 6-flavor strong coupling, see below. In contrast to the logarithmic μ_m evolution of $\overline{m}_t(\mu_m)$, the R -evolution of $m_t^{\text{MSR}}(R)$ is linear and captures the correct physical logarithms for observables with m_t dependence, generated at dynamical scales $R < m_t$, such as resonances, thresholds, and low-energy endpoints [46]. The mass renormalization constant of the MSR mass only contains the on-shell self-energy corrections for scales larger than R in contrast to the pole mass which contains self-energy corrections at all scales. So while the MSR mass is numerically close to the pole mass for small R at low orders, it is free of the pole mass renormalon problem. Formally the MSR mass approaches the pole mass for $R \rightarrow 0$, but the Landau pole prevents taking this limit in practice. For small R values in the range of 1 to 2 GeV the MSR mass captures the kinematic particle mass interpretation commonly associated of the pole mass. Within perturbative uncertainties at NLO, where we can still ignore the pole mass renormalon problem, the scheme choice $m_t^{\text{MSR}}(R = 1 \text{ GeV})$, or for some other very low value of R , is therefore a proxy for the pole mass scheme. The matching of the 5-flavor MSR mass to the 6-flavor $\overline{\text{MS}}$ mass at the scale $R = \overline{m}_t(\overline{m}_t)$ reads [13]

$$m_t^{\text{MSR}}(\overline{m}_t) = \overline{m}_t(\overline{m}_t) \left[1 + 0.10357 \left(a_s^{(5)}(\overline{m}_t) \right)^2 + 1.8308 \left(a_s^{(5)}(\overline{m}_t) \right)^3 \right], \quad (2.8)$$

and the inverse at the scale $R = m_t^{\text{MSR}}(m_t^{\text{MSR}})$ reads [13]

$$\overline{m}_t(\overline{m}_t) = m_t^{\text{MSR}}(m_t^{\text{MSR}}) \left[1 - 0.10357 \left(a_s^{(5)}(m_t^{\text{MSR}}) \right)^2 - 1.6927 \left(a_s^{(5)}(m_t^{\text{MSR}}) \right)^3 \right]. \quad (2.9)$$

²We are using the natural MSR mass definition (MSRn), where virtual top-quark loops are integrated out consistently, see [13].

The matching starts at $\mathcal{O}(\alpha_s^2)$, where virtual top quark loops first appear. In the matching relations in Eqs. (2.8) and (2.9) we have indicated the 5-flavor scheme for the strong coupling. At the order shown, the coefficients are identical to the ones in the 6-flavor scheme. These relations are in close analogy to the corresponding strong coupling matching relation which reads

$$a_s^{(6)}(\bar{m}_t) = a_s^{(5)}(\bar{m}_t) \left[1 - 0.15278 \left(a_s^{(5)}(\bar{m}_t) \right)^2 - 0.54881 \left(a_s^{(5)}(\bar{m}_t) \right)^3 \right]. \quad (2.10)$$

Note, the corrections to the matching relation shown in the brackets of Eq. (2.10) are known to $\mathcal{O}(\alpha_s^4)$ [47, 48]. The MSR mass at an arbitrary scale R is then obtained from a given $\overline{\text{MS}}$ mass, applying Eq. (2.8), and evolving the scale R from $\bar{m}_t(\bar{m}_t)$ to the desired value by solving the RGE

$$R \frac{d}{dR} m_t^{\text{MSR}}(R) = -R \sum_n \gamma_n^R \left(a_s^{(5)}(R) \right)^{n+1}, \quad (2.11)$$

where the anomalous dimensions γ_n^R are given by [45]

$$\begin{aligned} \gamma_0^R &= 4/3 \\ \gamma_1^R &= 3.0219, \\ \gamma_2^R &= 2.8047, \\ \gamma_3^R &= -73.257. \end{aligned} \quad (2.12)$$

The solution of Eq. (2.11) yields

$$m_t^{\text{MSR}}(\bar{m}_t) - m_t^{\text{MSR}}(R) = - \sum_{n=0} \gamma_n^R \int_R^{\bar{m}_t} dR' \left(a_s^{(5)}(R') \right)^{n+1} + \mathcal{O}(a_s^4) \equiv \Delta m, \quad (2.13)$$

so that the MSR mass at R is obtained as $m_t^{\text{MSR}}(R) = m_t^{\text{MSR}}(\bar{m}_t) - \Delta m$. As far as QCD corrections are concerned, the formulae above allow to relate MSR and $\overline{\text{MS}}$ top quark mass values at any (perturbative) scale with a precision of better than 20 MeV. The REvolver library [46] provides this functionality in a user-friendly software package.

In the present work, the MCFM program (version 6.8) [16, 17] is extended to include the implementation of the MSR scheme in the computation of the hadronic $t\bar{t}$ production cross section for single-differential kinematics. Based on the procedure presented in Refs. [18, 19], the $t\bar{t}$ production cross section differential with respect to an observable X at NLO reads

$$\begin{aligned} \frac{d\sigma}{dX} &= (a_s(\mu_r))^2 \frac{d\sigma^{(0)}}{dX}(m, \mu_r, \mu_f) + (a_s(\mu_r))^3 \frac{d\sigma^{(1)}}{dX}(m, \mu_r, \mu_f) \\ &+ (a_s(\mu_r))^3 \tilde{R} d_1 \frac{d}{dm_t} \left(\frac{d\sigma^{(0)}(m_t, \mu_r, \mu_f)}{dX} \right) \Big|_{m_t=m}, \end{aligned} \quad (2.14)$$

where $\sigma^{(0)}$ is the leading order (LO) and $\sigma^{(1)}$ the NLO cross section in the pole mass scheme. At NLO, the derivative term (the third summand in Eq. (2.14)) implements the $\overline{\text{MS}}$ or MSR top quark

mass schemes. In the present work, the observable of interest is the invariant mass of the $t\bar{t}$ system, and $X = m_{t\bar{t}}$. In particular, we have the following set of parameters in Eq. (2.14))

$$\left(a_s(\mu_r), m, d_1, \tilde{R}\right) = \begin{cases} \left(a_s^{(5)}(\mu_r), m_t^{\text{MSR}}(R), d_1^{\text{MSR}}, R\right), & R < \bar{m}_t(\bar{m}_t) \text{ (MSR regime)}, \\ \left(a_s^{(5)}(\mu_r), \bar{m}_t(\mu_m), d_1^{\overline{\text{MS}}}(\mu_m), \bar{m}_t(\mu_m)\right), & \mu_m > \bar{m}_t(\bar{m}_t) \text{ (}\overline{\text{MS}} \text{ regime)}. \end{cases} \quad (2.15)$$

It is important to note that the choice of the renormalization and factorization scales μ_r and μ_f is independent of the mass renormalization scales R or μ_m in this implementation. We emphasize that it is essential that the mass scheme correction proportional to d_1 is consistently used at the renormalization scale μ_r , which yields logarithms $\ln(R/\mu_r)$ or $\ln(\mu_m/\mu_r)$ beyond NLO to consistently cancel the pole mass renormalon. Since MCFM is based on renormalization with 5 dynamical flavors, one has to consistently expand $a_s^{(6)}(\mu_r)$ for the $\overline{\text{MS}}$ top mass scheme corrections of Eq. (2.1) in powers of $a_s^{(5)}(\mu_r)$ in the cross section formula of Eq. (2.14). At NLO this leads to Eq. (2.15).

We note that the fixed-order perturbative corrections for the differential cross section in the pole mass scheme are known at NNLO accuracy in QCD [25, 26] and at NLO in the electroweak theory [49, 50]. In addition, the $\overline{\text{MS}}$ mass scheme at NNLO has been studied in Ref. [51]. The conversion of the mass renormalization scheme from the pole mass to the $\overline{\text{MS}}$ or the MSR mass beyond NLO accuracy in QCD (and LO for electroweak effects as presented here) needs to be performed numerically and requires theory predictions for differential cross sections with the pole mass at NNLO accuracy for a large array of pole mass values (typically in a range $150 \text{ GeV} < m < 180 \text{ GeV}$). The required NNLO computations (including scale variations and PDF uncertainties) are numerically demanding and such results are currently not readily available in the literature.

Non-relativistic quasi-bound state QCD corrections are important for the region $m_{t\bar{t}} \sim 340\text{--}360 \text{ GeV}$, where the strongest top quark mass sensitivity arises in the $m_{t\bar{t}}$ distribution. In this threshold region the produced top quarks attain small non-relativistic velocities $v \ll 1$ in the $t\bar{t}$ center-of-mass frame, and the dynamics of the $t\bar{t}$ system are hence governed by the mass m_t , the relative momentum $m_t v$, and the kinetic energy $m_t v^2$ of the top quark. Since $m_t \gg m_t v \gg m_t v^2$, the appearance of ratios involving the masses, momenta and kinetic energy of the top quark renders the standard fixed-order expansion in powers of α_s unreliable in this $m_{t\bar{t}}$ range. The most pronounced quasi-bound state effects arise from the Coulomb corrections due to the exchange of gluons between the produced t and \bar{t} yielding a dependence of the prediction on the ratio $m_t/(m_t v)$. This leads to a singular $(\alpha_s/v)^n$ behavior in the fixed-order perturbative QCD correction at n -loops [52]. The quasi-bound state effects have been considered in Refs. [27, 28], and more recently again in [29]. For $t\bar{t}$ pairs in a color octet state, the effects of soft gluon exchanges with other parts of the hard production process can yield further significant corrections, which are currently unknown. The available predictions do not provide an adequate description of the lowest $m_{t\bar{t}}$ bin in the region between 300 GeV and the quasi-bound state region around 350 GeV, where the imaginary energy approach and the use of the optical theorem [14] predict a sizeable and unphysical finite

$t\bar{t}$ production rate, see the results shown in Ref. [29]. In this region the differential cross section depends on the experimental cuts on the top and antitop quark decay products [53, 54], which complicates the theoretical prediction as well as the experimental analysis, but any sensible choice of cuts leads to a strongly suppressed rate for $m_{t\bar{t}}$ close to 300 GeV. This latter aspect is actually better described by the fixed-order predictions for stable top quarks where the rate vanishes identically for $m_{t\bar{t}} < 2m_t$ (for a correct top mass scheme choice as discussed below). Furthermore, a systematic treatment of the intermediate region, where the non-relativistic and relativistic calculations need to be matched, is currently not available with a reliable matching error estimate.³ We also mention that for the electroweak corrections different scheme choices for the $\overline{\text{MS}}$ mass are available related to the definition of the vacuum expectation value [43, 44]. Their effects concerning the MSR mass and their impact on the use of different mass schemes in experimental observables are unknown. Overall, there is currently no complete and reliable theory prediction for the low $m_{t\bar{t}}$ distribution available for experimental analysis. For the study of the $t\bar{t}$ differential cross section as a function of $m_{t\bar{t}}$ and its dependence on the MSR mass scale R , the NLO fixed order prediction for stable top quarks based on the MCFM program is appropriate, since it properly describes the generic size of subleading QCD corrections and vanishes for $m_{t\bar{t}} < 2m_t$. For a reliable measurement of the MSR top quark mass, however, a more complete code including the features mentioned above has to be made available.

3 First investigation of the R scale dependence

In this section we examine the dependence of the $m_{t\bar{t}}$ distribution in different representative bins in the range between 300 and 700 GeV on the scales μ_r , μ_f , and R in the MSR mass scheme as well as μ_m in the $\overline{\text{MS}}$ scheme using as input the results of the ABMP16 PDF fit at NLO [56] with $\alpha_s^{(5)}(m_Z) = 0.11905$ at $m_Z = 91.19$ GeV. For the $\overline{\text{MS}}$ mass the value $\overline{m}_t(\overline{m}_t) = 160.68$ GeV has been chosen close to the fit of Ref. [57]. The latter value corresponds to MSR masses at $R = 1$ GeV and $R = 80$ GeV of $m_t^{\text{MSR}}(1 \text{ GeV}) = 170.48$ GeV and $m_t^{\text{MSR}}(80 \text{ GeV}) = 164.98$ GeV, respectively.

In Fig. 1, the cross section for the bin $m_{t\bar{t}} \in [300, 333]$ GeV, i.e. the region below the $t\bar{t}$ production threshold, is shown for different scale choices at LO and NLO. The cross section is zero for $R < 60$ GeV, which corresponds to $2m_t^{\text{MSR}}(R) > 333$ GeV. Non-zero contributions to the cross section in the $m_{t\bar{t}} \in [300, 333]$ GeV range appear only at large values of R or when using the $\overline{\text{MS}}$ mass, which correspond to smaller values of $m_t^{\text{MSR}}(R)$ or $\overline{m}_t(\mu_m)$. The LO contribution to the cross section is zero or positive throughout the probed range of R and μ_m . At NLO, however, the quick decrease of the derivative terms in Eq. (2.14) in comparison to the increase of the positive contributions would lead to unphysical negative values of the NLO cross section in this kinematic range, as was also pointed out in Ref. [51], where the $\overline{\text{MS}}$ mass scheme was examined.

Since $t\bar{t}$ production in the range $m_{t\bar{t}} \in [300, 333]$ GeV is impossible, the results in Fig. 1 also show that R values above 80 GeV must be avoided. This also implies that the $\overline{\text{MS}}$ mass cannot be

³Such a treatment is available only for top quark production in e^+e^- annihilation, see Ref. [55].

used if the $t\bar{t}$ cross section in this $m_{t\bar{t}}$ range is included in the experimental analysis. This conclusion holds even in the presence of quasi-bound state effects, since these provide a more precise prediction of the $t\bar{t}$ production threshold, which is, however, located at $m_{t\bar{t}}$ values above 333 GeV. A further feature of the $m_{t\bar{t}} \in [300, 333]$ GeV range, shown in Fig. 1, is the rapid increase of the cross section at $\mu_m \gtrsim 410$ GeV. This occurs when $\bar{m}_t(\mu_m)$ is so small, such that LO $t\bar{t}$ production is even possible below 300 GeV.

In Fig. 2, the cross section for the bin $m_{t\bar{t}} \in [333, 366]$ GeV, i.e. the region where the $t\bar{t}$ production threshold is located, is shown as a function of R and μ_m at NLO in the left panel. The right panel displays the relative size of the NLO corrections with respect to the LO description. Here, the quasi-bound state effects already contained in the NLO prediction are sizeable and our NLO result only provides a qualitative description. Similar as in the lowest bin, we observe a quite strong dependence on the mass renormalization scale. We see that for very small values of R the size of the NLO correction increases significantly, particularly for large μ_r and μ_f values, making the use of fixed-order perturbation theory unreliable for these choices. This shows that the impact of the higher-order QCD corrections, including the quasi-bound state corrections, is particularly sizeable and essentially maximized in the pole mass scheme. This is closely mimicked by the result for $R = 1$ GeV.

On the other hand, with increasing R , the impact of the NLO corrections decreases substantially. This is illustrated in the right panel of Fig. 2, where the ratio of cross sections at NLO to that at LO is shown to be closer to unity. This should be interpreted as the NLO corrections being small at these R . Particularly, with R in the range 60 GeV to 80 GeV, the cross section remains robust

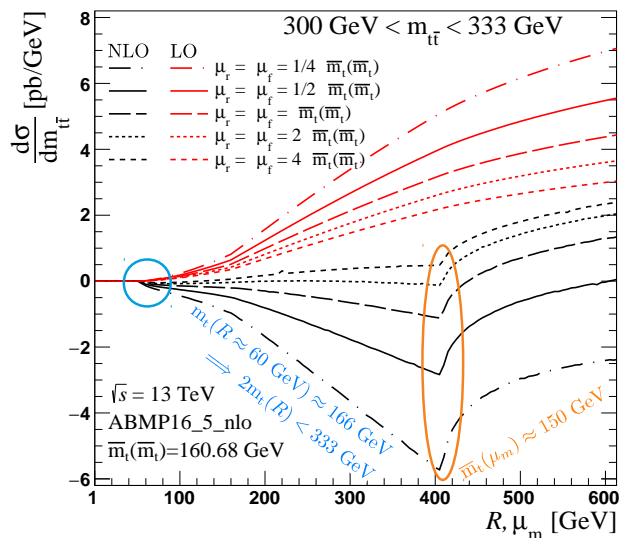


Figure 1: The $m_{t\bar{t}} \in [300, 333]$ GeV range of the $m_{t\bar{t}}$ distribution. There is no $t\bar{t}$ production at $R \lesssim 60$ GeV, but the region above it suffers from the lack of Coulomb corrections. The discontinuity at $\mu_m \gtrsim 410$ GeV is due to the $t\bar{t}$ production threshold becoming artificially low, and such high values of the scale μ_m should be avoided.

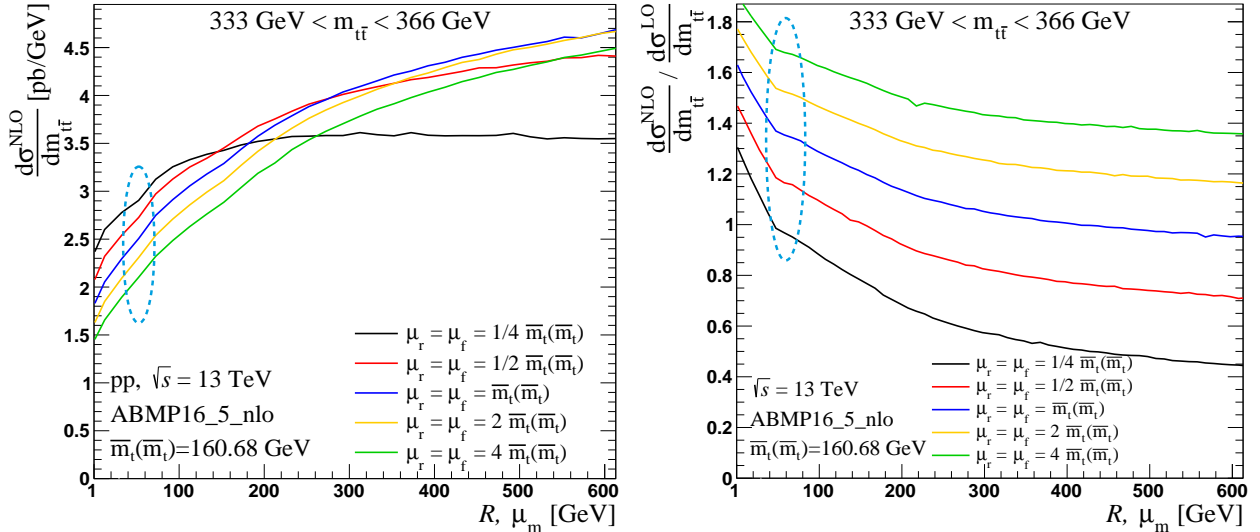


Figure 2: The NLO cross section (left) and the ratio of the LO and NLO cross sections (right) for $m_{t\bar{t}} \in [333, 366]$ GeV. The transition from a region suffering from the missing Coulomb corrections to a more stable region where the threshold effects become less important is seen at $R \gtrsim 60$ GeV (dashed blue). Further, predictions obtained using small values of μ_r , μ_f are observed to stabilize the prediction quickly as a function of R or μ_m .

under variations of all the scales: it changes only little as a function of R , while the differences between the curves corresponding to smaller or larger central values for μ_r and μ_f remain small. This is not accidental, but expected from the fact that the smaller value of the MSR mass at larger R values accounts for the fact that the mass of the $t\bar{t}$ system is reduced on average by the Coulomb-binding effects. Therefore, with R in the range 60 GeV to 80 GeV, also the impact of the (missing) Coulomb corrections can be expected to be moderate and in particular much smaller than they would be for very small values of R , which serve as a proxy for the pole mass scheme. It is also observed that setting μ_r and μ_f to values below the top quark mass further diminishes the size of the NLO corrections. The reason is that for this particular R -range and chosen μ_r and μ_f , $m_t^{\text{MSR}}(R)$ captures a sizable part of the non-relativistic bound-state dynamics relevant in the region $m_{t\bar{t}} \in [333, 366]$ GeV. In other words, a significant part of the binding effects is already absorbed into the mass value, so that the fixed-order prediction at NLO in the MSR scheme provides a more precise description of the process as compared to the pole mass scheme. Considering the observations in the $m_{t\bar{t}}$ range of [300, 366] GeV (Fig. 1 and Fig. 2), it can be concluded that the most stable predictions are obtained for R in the range of 60 to 80 GeV. Out of this range, the highest choice for the scale, $R = 80$ GeV is preferred as the default choice, to avoid entering the regime of $R < 60$ GeV while allowing the examination of the R scale variation uncertainties, see Sec. 4. From the experience gained in studies of the $t\bar{t}$ threshold scan at e^+e^- -colliders [14] one may expect that a MSR mass scale $R \sim 25$ GeV should be more appropriate. However, due to the integration over the $m_{t\bar{t}}$ range, the values of R and μ_r need to be larger, than those used to describe

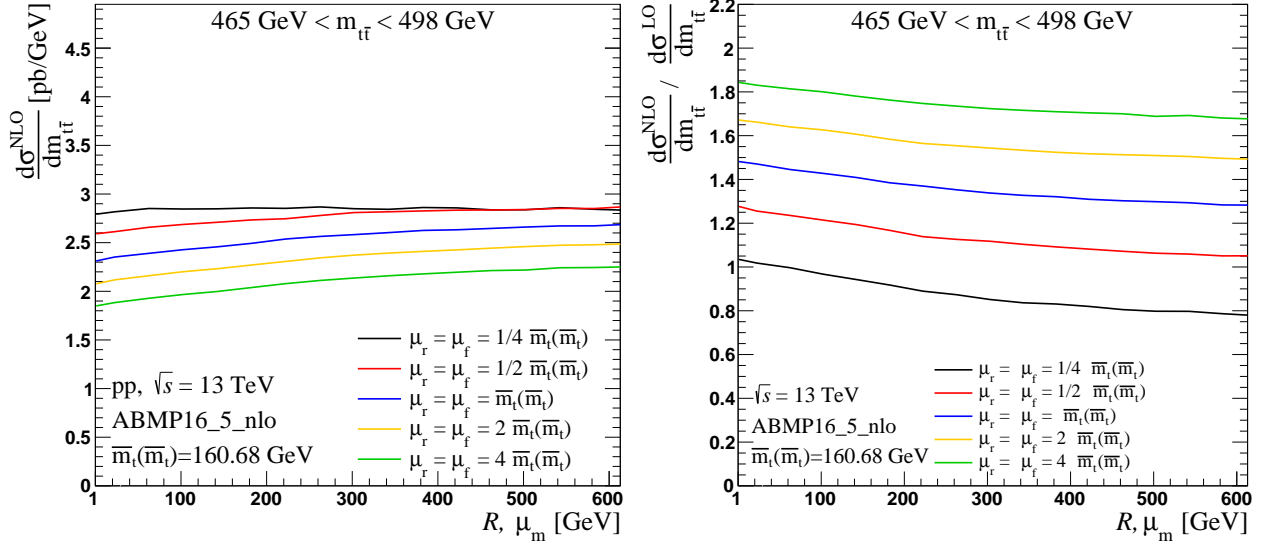


Figure 3: The NLO cross section (left) and the ratio of the LO and NLO cross sections (right) for $m_{t\bar{t}} \in [465, 498]$ GeV.

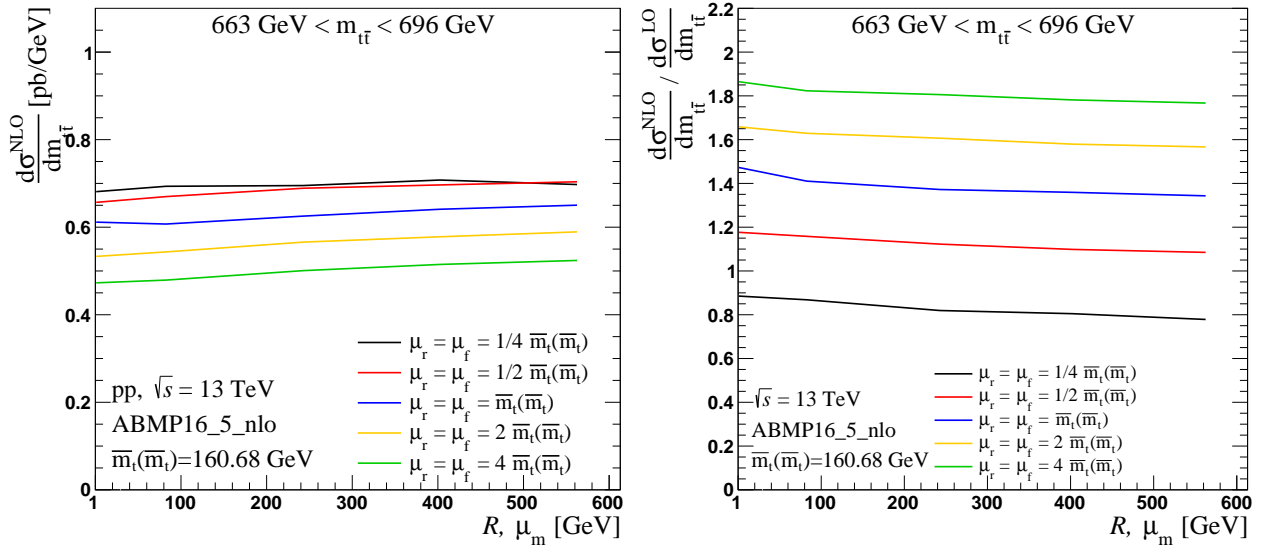


Figure 4: Same as Fig. 3 for the bin $m_{t\bar{t}} \in [663, 696]$ GeV.

the peak of the bound-state resonance, corresponding to a much narrower $m_{t\bar{t}}$ distribution.

At this point it is also instructive to examine $m_{t\bar{t}}$ far above threshold. In Figs. 3 and 4, the results for $m_{t\bar{t}} \in [465, 498]$ GeV and $m_{t\bar{t}} \in [663, 696]$ GeV, respectively, are shown. Here the NLO predictions provide an appropriate theoretical description. In contrast to the low $m_{t\bar{t}}$ bins discussed above, the mass renormalization scale behavior is very smooth. This is partly related to the much smaller top quark mass sensitivity, but also means that none of the top quark mass schemes (and values for R or μ_m) provide any advantage concerning capturing essential QCD corrections. Here,

only the choices of the scales μ_r and μ_f are essential for the prediction showing a preference for values of around m_t . This observation applies also to other invariant mass bins covering large $m_{t\bar{t}}$ values, see Ref. [58].

Overall, our examination suggests that the MSR top quark mass $m_t^{\text{MSR}}(R)$ and the choice for the central value of $R = 80$ GeV provide the most reliable theoretical predictions for all $m_{t\bar{t}}$ bins. For the scales μ_r and μ_f the central values $\bar{m}_t(\bar{m}_t)$ and, in particular $\bar{m}_t(\bar{m}_t)/2$ for the $m_{t\bar{t}}$ range containing the $t\bar{t}$ threshold, are adequate choices. We note that these findings are also in line with the optimal scale choices for the total cross section for $t\bar{t}$ hadro-production, when using the top quark mass in the $\overline{\text{MS}}$ scheme. In this case, central values for μ_r and μ_f of the order $\bar{m}_t(\bar{m}_t)/2 \approx 80$ GeV are in the region of fastest apparent convergence considering perturbative QCD corrections through NNLO and also minimize the scale sensitivity of the total cross section [19]. Settings for PDF factorization scale μ_f different from μ_r have been explored in Refs [24, 51], corroborating these findings. On the other hand, for the total cross section with the top quarks in the pole mass scheme, which is well modeled by the MSR scheme mass $m_t^{\text{MSR}}(1 \text{ GeV})$, the preferred central values for μ_r and μ_f , which minimize scale sensitivity and optimize perturbative convergence through NNLO, are of the order $m_t^{\text{pole}}/4 \approx 45$ GeV, see e.g. Ref. [19]. This is also visible in the ratio plots on the right in Figs. 2–4. In the following, we demonstrate the impact of the mass scheme and the scale setting on the value of the top quark mass obtained in fits to the experimental data of Ref. [15].

4 Extraction of the top quark MSR mass

The MSR mass $m_t^{\text{MSR}}(R)$ is extracted from the differential $t\bar{t}$ production cross section measured by the CMS Collaboration in pp collisions at the LHC at $\sqrt{s} = 13$ TeV, corresponding to an integrated luminosity of 35.9 fb^{-1} [15]. The $t\bar{t}$ cross section is measured as a function of $m_{t\bar{t}}$ in the ranges: $m_{t\bar{t}} < 420$ GeV, $m_{t\bar{t}} \in [420, 550]$ GeV, $m_{t\bar{t}} \in [550, 810]$ GeV and $m_{t\bar{t}} > 810$ GeV.

The theoretical predictions are obtained using the ABMP16 5-flavor PDF set [57] at NLO. According to the preferred MSR mass scale settings described in the previous section, the initial value of the scale R is set to 80 GeV in Eq. (2.14), and the cross section is calculated for a range of assumed values of $m_t^{\text{MSR}}(80 \text{ GeV})$. The function

$$\chi^2 = \sum_{i,j} (\sigma_i^{\text{exp}} - \sigma_i^{\text{th}}) C_{ij}^{-1} (\sigma_j^{\text{exp}} - \sigma_j^{\text{th}}), \quad (4.1)$$

is computed for each $m_t^{\text{MSR}}(80 \text{ GeV})$. The indices i, j in Eq. (4.1) run over the bins of the $m_{t\bar{t}}$ distribution, while σ_i^{exp} are the experimental data and σ_i^{th} the theoretical predictions. The inverse covariance matrix C_{ij}^{-1} provided in Ref. [15] is used.

The scales μ_r and μ_f are set to $m_t^{\text{MSR}}(80 \text{ GeV})$ for all 4 bins of the $m_{t\bar{t}}$ distribution or, alternatively, to $m_t^{\text{MSR}}(80 \text{ GeV})/2$ for $m_{t\bar{t}} < 420$ GeV, to stabilize the prediction against the missing quasi-bound state corrections, and to $m_t^{\text{MSR}}(80 \text{ GeV})$ for the remainder. Fig. 5 shows a 4th order polynomial fit to the χ^2 values resulting from each configuration.

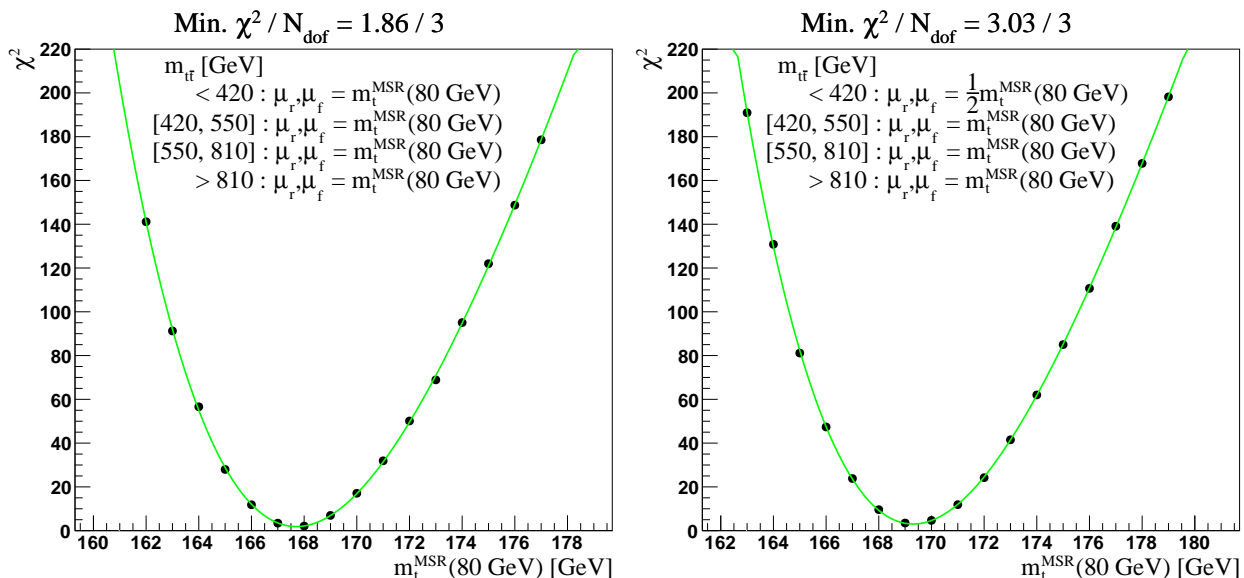


Figure 5: A 4th order polynomial fitted to the χ^2 resulting from comparing the experimental data to theory predictions assuming different values of $m_t^{\text{MSR}}(80 \text{ GeV})$. The scales μ_r and μ_f are set to $m_t^{\text{MSR}}(80 \text{ GeV})$ considering the whole $m_{t\bar{t}}$ distribution (left), or to $m_t^{\text{MSR}}(80 \text{ GeV})/2$ for $m_{t\bar{t}} < 420 \text{ GeV}$ and to $m_t^{\text{MSR}}(80 \text{ GeV})$ for the remainder (right). The number of degrees of freedom in the fits is denoted by N_{dof} .

The fit uncertainties are obtained via the $\Delta\chi^2 = 1$ tolerance criterion, while the μ_r and μ_f scale uncertainties are evaluated by varying their central values in each bin up and down by a factor of 2, avoiding the cases where one scale is multiplied by 1/2 and the other by 2, and constructing an envelope. For comparison with previous analyses, the extracted values of $m_t^{\text{MSR}}(80 \text{ GeV})$ are evolved to the reference scales R of 1 and 3 GeV. Note that determining $m_t^{\text{MSR}}(1 \text{ GeV})$ requires evaluating $\alpha_s(1 \text{ GeV})$ rather close to the Landau pole, which is expected to lead to an increased perturbative uncertainty in the MSR mass at $R = 1 \text{ GeV}$ due to missing higher order corrections. Reporting the mass value also at $R = 3 \text{ GeV}$ thus ensures the stability of the result, and the use of reference scales $R > 1 \text{ GeV}$ will become increasingly important in future extractions of $m_t^{\text{MSR}}(R)$. Furthermore, the results are translated into the standard $\overline{\text{MS}}$ mass $\overline{m}_t(\overline{m}_t)$ by iteratively finding $m_t^{\text{MSR}}(m_t^{\text{MSR}})$ via the condition $R = m_t^{\text{MSR}}(R)$, and applying the matching formula in Eq. (2.9) up to $\mathcal{O}(a_s^3)$. The uncertainty related to the initial choice of R is assessed by repeating the fits at $R = 60 \text{ GeV}$ and $R = 100 \text{ GeV}$, and the difference in the resulting masses at the reference scales to the respective values obtained in the $R = 80 \text{ GeV}$ fit is taken as the R scale uncertainty. The resulting values for the top quark mass are listed in Table 1.

In particular, setting the central μ_r and μ_f to $m_t^{\text{MSR}}(80 \text{ GeV})$ and considering the complete $m_{t\bar{t}}$ distribution yields

$$m_t^{\text{MSR}}(1 \text{ GeV}) = 173.2 \pm 0.6 (\text{fit})_{-0.6}^{+0.4} (\mu_r, \mu_f)_{-0.5}^{+0.4} (R) \text{ GeV}. \quad (4.2)$$

The value for $m_t^{\text{MSR}}(80 \text{ GeV})$ in this fit translates into $\overline{m}_t(\overline{m}_t) = 163.3_{-1.0}^{+0.8} \text{ GeV}$. This is compatible

Table 1: The values of $m_t^{\text{MSR}}(R)$ obtained at different scales R (given in brackets below m_t^{MSR}), and the corresponding $\bar{m}_t(\bar{m}_t)$, the χ^2 divided by the number of degrees of freedom N_{dof} in the fit, along with the fit and scale uncertainties for the $m_t^{\text{MSR}}(R)$ extracted at $R = 80$ GeV. The results are shown for the constant μ_r, μ_f setting, where the central μ_r and μ_f values are set to $m_t^{\text{MSR}}(80 \text{ GeV})$ in the whole $m_{t\bar{t}}$ distribution, and for the semi-dynamical (SD) setting where they are set to $m_t^{\text{MSR}}(80 \text{ GeV})/2$ for $m_{t\bar{t}} < 420$ GeV and to $m_t^{\text{MSR}}(80 \text{ GeV})$ for higher $m_{t\bar{t}}$. The fit and μ_r, μ_f uncertainties correspond to the MSR mass extracted at $R = 80$ GeV. Within the reported accuracy, the uncertainty in the initial choice of R agrees in all cases when the extracted $m_t^{\text{MSR}}(R)$ is evolved to the reference R .

μ_r, μ_f setting	χ^2/N_{dof}	$m_t^{\text{MSR}}(80 \text{ GeV})$ [GeV]	$m_t^{\text{MSR}}(1 \text{ GeV})$ [GeV]	$m_t^{\text{MSR}}(3 \text{ GeV})$ [GeV]	$\bar{m}_t(\bar{m}_t)$ [GeV]	Fit unc. [GeV]	μ_r, μ_f unc. [GeV]	R unc. [GeV]
Const.	1.86/3	167.7	173.2	172.9	163.3	+0.6 -0.6	+0.4 -0.6	+0.4 -0.5
SD	3.03/3	169.3	174.8	174.5	164.8	+0.5 -0.5	+0.2 -0.4	+0.2 -0.3

within uncertainties with the value of $\bar{m}_t(\bar{m}_t) = 162.1_{-1.0}^{+1.0}$ GeV obtained at NLO in the ABMP16 5-flavor PDF set [56].

In accordance with the results shown in Fig. 1, multiplying the scales μ_r and μ_f by 1/2 within $m_{t\bar{t}} < 420$ GeV is observed to increase the NLO cross section at $R = 80$ GeV. To compensate for this effect, the fit for $m_t^{\text{MSR}}(80 \text{ GeV})$ leads to a somewhat larger value for the top quark MSR mass, reducing the predicted cross section especially in the vicinity of the $t\bar{t}$ production threshold. This results in the value

$$m_t^{\text{MSR}}(1 \text{ GeV}) = 174.8 \pm 0.5 (\text{fit})_{-0.4}^{+0.2} (\mu_r, \mu_f)_{-0.3}^{+0.2} (R) \text{ GeV}. \quad (4.3)$$

It is expected that the impact of the choices for μ_r and μ_f , i.e. the shift of 1.6 GeV in the central values between Eqs. (4.2) and (4.3), will be reduced at NNLO accuracy and once a reliable description of the quasi-bound state effects is available. Nonetheless, as anticipated from the observations in Sec. 3, the scale setting in Eq. (4.3) already increases the robustness against scale variations, yielding somewhat smaller uncertainties than Eq. (4.2). Even though one may consider the 1.6 GeV difference as a quantification of the uncertainty of our current NLO analysis, a proper uncertainty analysis should include the NNLO and quasi-bound state corrections as well as order dependent input quantities (including PDFs, the strong coupling and their correlation) and is postponed to future work.

In order to illustrate the main conceptual novelty and the phenomenological importance of the mass scheme choice, we also perform the following variant of the fit: Instead of determining the top quark MSR mass at $R = 80$ GeV and evolving the extracted $m_t^{\text{MSR}}(80 \text{ GeV})$ value to $R = 1$ GeV, as in Eqs. (4.2) and (4.3), we perform the fit to data directly with the initial scale set to $R = 1$ GeV in NLO cross section of Eq. (2.14). Using also the central scales μ_r, μ_f set to $m_t^{\text{MSR}}(1 \text{ GeV})$, this results in

$$m_t^{\text{MSR}}(1 \text{ GeV}) = 170.1 \pm 0.6 (\text{fit})_{-0.9}^{+1.1} (\mu_r, \mu_f) \text{ GeV}, \quad (4.4)$$

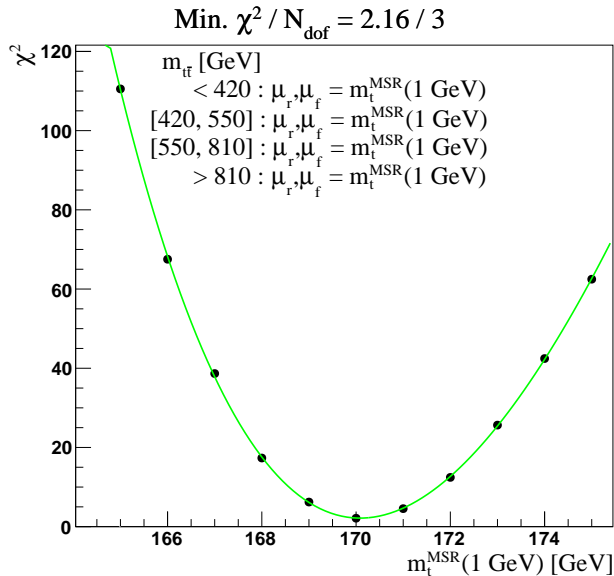


Figure 6: Same as Fig. 5, now fitting $m_t^{\text{MSR}}(1 \text{ GeV})$ and with the scales μ_r and μ_f set to $m_t^{\text{MSR}}(1 \text{ GeV})$ in the whole $m_{t\bar{t}}$ distribution.

where the corresponding fit to χ^2 is shown in Fig. 6. In Eq. (4.4) the μ_r and μ_f scale uncertainties are twice as large as those of Eq. (4.2). The even more sizeable discrepancy to the results of Eqs. (4.2) and (4.3) indicates that scale variation does not provide a proper estimate of the theoretical uncertainties due to the missing higher order and quasi-bound state corrections for the result quoted in Eq. (4.4). Since using $m_t^{\text{MSR}}(1 \text{ GeV})$ closely approximates the outcome using pole mass scheme, this confirms our conclusions drawn in Sec. 3 that the use of the pole mass scheme (or a very small initial R value for the MSR mass) leads to less reliable results in a fixed order QCD description at NLO accuracy, where the resummation of the quasi-bound state effects is missing. The significant difference of 4.7 GeV between the central values in Eqs. (4.3) and (4.4), as compared to the quoted scale uncertainties, demonstrates the phenomenological relevance of this issue. This underpins the importance of an adequate top mass scheme choice as well as a proper scale setting in future m_t extractions based on the $m_{t\bar{t}}$ measurements.

Let us now comment on other recent extractions of the top-quark mass, which have employed different methodologies. Data from the CMS Collaboration for the $t\bar{t}$ production cross section collected in pp collisions at the LHC at $\sqrt{s} = 13 \text{ TeV}$ have been used previously for a determination of the top-quark mass using both, the pole and the $\overline{\text{MS}}$ mass scheme [20, 59]. The emphasis of those analyses has been on keeping the correlations of the top-quark mass with the strong coupling $\alpha_s(m_Z)$ and the PDFs. In a different thread of analyses, the running of top quark $\overline{\text{MS}}$ mass $\overline{m}_t(\mu_m)$ has been studied at NLO [15] and NNLO [60] with dynamical scales, using data from the CMS Collaboration for the $m_{t\bar{t}}$ distributions.⁴

⁴See also http://cms-results.web.cern.ch/cms-results/public-results/publications/TOP-19-007/index.html#Figure-aux_001.

Of these analyses, the results of Ref. [20] can be compared to the present work, since they are obtained from normalized multi-differential cross sections which also include the low $m_{t\bar{t}}$ region discussed here, and the theoretical predictions are also based on the NLO MCFM cross section description. Ref. [20] quotes $m_t^{\text{pole}} = 170.5 \pm 0.8 \text{ GeV}$, which, if interpreted as the asymptotic pole mass [46], translates into $m_t^{\text{MSR}}(1 \text{ GeV}) = 170.2 \pm 0.8 \text{ GeV}$. This is compatible with the variant of the present study in Eq. (4.4) obtained by directly fitting $m_t^{\text{MSR}}(1 \text{ GeV})$ to data, although the combined fit of m_t^{pole} , $\alpha_s(m_Z)$ and PDFs in Ref. [20] reports a smaller value of $\alpha_s(m_Z)$ than used in Eq. (4.4) on the basis of the ABMP16 PDF set, and a somewhat different gluon PDF. The result of Ref. [20] is systematically lower than those obtained using inclusive $t\bar{t}$ cross section measurements [21–23]. The results of our analyses shown in Eqs. (4.2) and (4.3) demonstrate that a larger and more reliable value could be obtained once the quasi-bound state, and potentially also NNLO corrections, are accounted for.

The value for the top quark MSR mass of $m_t^{\text{MSR}}(3 \text{ GeV}) = 169.6_{-1.1}^{+0.8} \text{ GeV}$, which corresponds to $m_t^{\text{MSR}}(1 \text{ GeV}) = 169.9_{-1.1}^{+0.8} \text{ GeV}$, has been extracted in Ref. [24], using the CMS data of Ref. [20] and the same methodology, i.e. using fixed-order QCD perturbation theory at NLO accuracy, so that $m_t^{\text{MSR}}(3 \text{ GeV})$ has been fitted simultaneously with the PDFs and strong coupling constant. Evolving the result of the present study in Eq. (4.3) to $R = 3 \text{ GeV}$ yields

$$m_t^{\text{MSR}}(3 \text{ GeV}) = 174.5 \pm 0.5 (\text{fit})_{-0.4}^{+0.2} (\mu_r, \mu_f)_{-0.3}^{+0.2} (R) \text{ GeV}, \quad (4.5)$$

which indicates some tension as well.⁵ The result of Ref. [24] is very close to the one obtained in Ref. [20] because using the MSR mass with a very low R results in a value very close to the pole mass, as discussed above. The result obtained for the MSR mass $m_t^{\text{MSR}}(3 \text{ GeV})$ in Ref. [24] and the differences obtained in our analyses shown in Eq. (4.4) in comparison to Eqs. (4.2) and (4.3) underline that just using the MSR mass $m_t^{\text{MSR}}(R)$ instead of the pole mass may not lead to a different result at all if the scale R is not chosen in an adequate way. Further, Ref. [24] has obtained $\alpha_s(m_Z) = 0.1132_{-0.0018}^{+0.0023}$, which is two standard deviations away from the value of the ABMP16 fit at NLO [56] used in the extraction of Eq. (4.5). The similar values of $m_t^{\text{MSR}}(3 \text{ GeV})$ in Ref. [24] and in Eq. (4.4) indicate a less significant impact of the value of $\alpha_s(m_Z)$ on the m_t extraction for the observable under consideration. A related observation was made for the top quark mass sensitivity in the 2-jettiness distribution analyzed in Refs. [61] for boosted top pair production e^+e^- collisions.

Notably, neither any of the cited previous top quark mass extractions based on the LHC data nor the present work have included the aforementioned corrections for the quasi-bound state effects. However, the extraction of the top quark MSR mass using predictions in the MSR scheme at the scale $R = 80 \text{ GeV}$ profits from the smaller size of these effects and thus from an improved stability of the cross section.

We note that the ATLAS Collaboration has derived a value for the top quark MSR mass at the

⁵The computations in Ref. [24] rely on the practical MSR (pMSR) definition [13] instead of the natural MSR (nMSR) scheme used in this work. The difference is at the level of 10 MeV [13] and thus negligible for the uncertainties quoted.

reference scale $R = 1 \text{ GeV}$ in Ref. [30] by comparing QCD predictions at next-to-leading logarithmic accuracy for the soft-drop groomed top quark jet mass distribution to parton shower Monte Carlo simulations for a Monte-Carlo top quark mass $m_t^{\text{MC}} = 172.5 \text{ GeV}$. Obtained in the Monte Carlo calibration (following [61]), the result of Ref. [30] is not based on experimental data and hence cannot be directly compared to the results of the present study.

5 Summary and Conclusions

We have presented the first comprehensive study of the $m_{t\bar{t}}$ distribution in its dependence on the mass renormalization scales R and μ_m of the MSR and $\overline{\text{MS}}$ top quark mass schemes. Our findings suggest that using the MSR mass $m_t^{\text{MSR}}(R)$ with the scale setting of R close to 80 GeV improves the robustness of the predictions for the $m_{t\bar{t}}$ distribution against scale variations in general and, in particular, against the impact of quasi-bound state corrections in the region of $m_{t\bar{t}}$ close to the $t\bar{t}$ threshold. The theory predictions used in our study are based on the NLO fixed order QCD description provided by the MCFM program, adapted to the MSR and $\overline{\text{MS}}$ top quark mass schemes. The optimized scale choices for those mass schemes are characterized by low values of the renormalization and factorization scales μ_r and μ_f . This holds in particular in the vicinity of the $t\bar{t}$ production threshold region in the $m_{t\bar{t}}$ distribution, where values $\mu_r \simeq \mu_f \simeq m_t/2$ are observed to stabilize cross section predictions and to decrease the scale uncertainty in the determination of the MSR mass.

These settings have been applied in an extraction of the top quark MSR mass at $R = 80 \text{ GeV}$, using $t\bar{t}$ pair production cross section, measured as a function of $m_{t\bar{t}}$ in pp collisions at $\sqrt{s} = 13 \text{ TeV}$ at the LHC by the CMS Collaboration, using fixed-order perturbative QCD predictions at NLO accuracy and also the semi-dynamical scales for μ_r , μ_f in the low- $m_{t\bar{t}}$ regime. The fitted value of $m_t^{\text{MSR}}(80 \text{ GeV})$ has then been evolved to various low reference scales R , rather than computing the cross sections directly at low R as performed in earlier analyses. This procedure yields the value $m_t^{\text{MSR}}(3 \text{ GeV}) = 174.5_{-0.7}^{+0.6} \text{ GeV}$, which is discussed in the context of other recent extractions of the top quark mass from LHC data. The observed differences are explained to a large part by the scale choice of $R = 80 \text{ GeV}$ for the top quark MSR mass, advocated by the present study, signifying the achieved systematic resummation of higher order QCD corrections. Other reasons for differences are due to the choice of the value for the strong coupling $\alpha_s(m_Z)$, which directly affects the normalization of the cross section and is anti-correlated with the top quark mass, and, to a lesser extent, due to the particular PDF sets used.

While we have argued that the implementation of the MSR mass scheme in the $t\bar{t}$ cross section calculation and the optimal scale choice for R of 80 GeV provide more robust predictions even at NLO accuracy, the findings should be corroborated by extending the analysis to NNLO accuracy. In addition, the proper treatment of both, the quasi-bound state effects, together with a matching to the relativistic $t\bar{t}$ region, and the $m_{t\bar{t}}$ region below the threshold are further important improvements to be implemented. A final reliable measurement of the top quark MSR mass needs to address those

issues as well as the correlation of the top quark mass with the other theoretical parameters, which control the cross section predictions. We leave these aspects for future studies.

Acknowledgements

The work of A.H.H was supported in part by FWF Austrian Science Fund under the Project No. P32383-N27, the work of S.M. in part by the Bundesministerium für Bildung und Forschung under contract 05H21GUCCA, the work by T.M. and K. L. is supported by the Helmholtz Association under the contract W2/W3-123, and T.M. is also supported by the National Science Centre, Poland, research grant No. 2021/42/E/ST2/00031.

References

- [1] F. Bezrukov et al. “Higgs Boson Mass and New Physics”. In: *JHEP* 10 (2012), p. 140. arXiv: 1205.2893 [hep-ph].
- [2] G. Degrandi et al. “Higgs mass and vacuum stability in the Standard Model at NNLO”. In: *JHEP* 08 (2012), p. 098. arXiv: 1205.6497 [hep-ph].
- [3] S. Alekhin, A. Djouadi, and S. Moch. “The top quark and Higgs boson masses and the stability of the electroweak vacuum”. In: *Phys. Lett. B* 716 (2012), pp. 214–219. arXiv: 1207.0980 [hep-ph].
- [4] A. V. Bednyakov et al. “Stability of the Electroweak Vacuum: Gauge Independence and Advanced Precision”. In: *Phys. Rev. Lett.* 115.20 (2015), p. 201802. arXiv: 1507.08833 [hep-ph].
- [5] I. I. Y. Bigi et al. “The Pole mass of the heavy quark. Perturbation theory and beyond”. In: *Phys. Rev. D* 50 (1994), pp. 2234–2246. arXiv: hep-ph/9402360.
- [6] M. Beneke and V. M. Braun. “Heavy quark effective theory beyond perturbation theory: Renormalons, the pole mass and the residual mass term”. In: *Nucl. Phys. B* 426 (1994), pp. 301–343. arXiv: hep-ph/9402364.
- [7] M. C. Smith and S. S. Willenbrock. “Top quark pole mass”. In: *Phys. Rev. Lett.* 79 (1997), pp. 3825–3828. arXiv: hep-ph/9612329.
- [8] S. Ferrario Ravasio, P. Nason, and C. Oleari. “All-orders behaviour and renormalons in top-mass observables”. In: *JHEP* 01 (2019), p. 203. arXiv: 1810.10931 [hep-ph].
- [9] A. H. Hoang. “What is the Top Quark Mass?” In: *Ann. Rev. Nucl. Part. Sci.* 70 (2020), pp. 225–255. arXiv: 2004.12915 [hep-ph].
- [10] G. ’t Hooft. “Dimensional regularization and the renormalization group”. In: *Nucl. Phys. B* 61 (1973), pp. 455–468.
- [11] W. A. Bardeen et al. “Deep-inelastic scattering beyond the leading order in asymptotically free gauge theories”. In: *Phys. Rev. D* 18 (11 Dec. 1978), pp. 3998–4017. URL: <https://link.aps.org/doi/10.1103/PhysRevD.18.3998>.
- [12] A. H. Hoang et al. “Infrared Renormalization Group Flow for Heavy Quark Masses”. In: *Phys. Rev. Lett.* 101 (2008), p. 151602. arXiv: 0803.4214 [hep-ph].

- [13] A. H. Hoang et al. “The MSR mass and the $\mathcal{O}(\Lambda_{\text{QCD}})$ renormalon sum rule”. In: *JHEP* 04 (2018), p. 003. arXiv: 1704.01580 [hep-ph].
- [14] A. H. Hoang et al. “Top - anti-top pair production close to threshold: Synopsis of recent NNLO results”. In: *Eur. Phys. J. direct* 2.1 (2000), p. 3. arXiv: hep-ph/0001286.
- [15] A. M. Sirunyan et al. “Running of the top quark mass from proton-proton collisions at $\sqrt{s} = 13\text{TeV}$ ”. In: *Phys. Lett. B* 803 (2020), p. 135263. arXiv: 1909.09193 [hep-ex].
- [16] J. M. Campbell and R. K. Ellis. “MCFM for the Tevatron and the LHC”. In: *Nucl. Phys. B Proc. Suppl.* 205-206 (2010). Ed. by J. Blümlein, S.-O. Moch, and T. Riemann, pp. 10–15. arXiv: 1007.3492 [hep-ph].
- [17] J. M. Campbell and R. K. Ellis. “Top-Quark Processes at NLO in Production and Decay”. In: *J. Phys. G* 42.1 (2015), p. 015005. arXiv: 1204.1513 [hep-ph].
- [18] U. Langenfeld, S. Moch, and P. Uwer. “Measuring the running top-quark mass”. In: *Phys. Rev. D* 80 (2009), p. 054009. arXiv: 0906.5273 [hep-ph].
- [19] M. Dowling and S. Moch. “Differential distributions for top-quark hadro-production with a running mass”. In: *Eur. Phys. J. C* 74.11 (2014), p. 3167. arXiv: 1305.6422 [hep-ph].
- [20] A. M. Sirunyan et al. “Measurement of $t\bar{t}$ normalised multi-differential cross sections in pp collisions at $\sqrt{s} = 13\text{ TeV}$, and simultaneous determination of the strong coupling strength, top quark pole mass, and parton distribution functions”. In: *Eur. Phys. J. C* 80.7 (2020), p. 658. arXiv: 1904.05237 [hep-ex].
- [21] G. Aad et al. “Determination of the top-quark pole mass using $t\bar{t} + 1\text{-jet}$ events collected with the ATLAS experiment in 7 TeV pp collisions”. In: *JHEP* 10 (2015), p. 121. arXiv: 1507.01769 [hep-ex].
- [22] G. Aad et al. “Measurement of the top-quark mass in $t\bar{t} + 1\text{-jet}$ events collected with the ATLAS detector in pp collisions at $\sqrt{s} = 8\text{ TeV}$ ”. In: *JHEP* 11 (2019), p. 150. arXiv: 1905.02302 [hep-ex].
- [23] “Measurement of the top quark pole mass using $t\bar{t} + \text{jet}$ events in the dilepton final state in proton-proton collisions at $\sqrt{s} = 13\text{ TeV}$ ”. In: (July 2022). arXiv: 2207.02270 [hep-ex].
- [24] M. V. Garzelli et al. “Heavy-flavor hadro-production with heavy-quark masses renormalized in the $\overline{\text{MS}}$, MSR and on-shell schemes”. In: *JHEP* 04 (2021), p. 043. arXiv: 2009.07763 [hep-ph].
- [25] M. Czakon, D. Heymes, and A. Mitov. “High-precision differential predictions for top-quark pairs at the LHC”. In: *Phys. Rev. Lett.* 116.8 (2016), p. 082003. arXiv: 1511.00549 [hep-ph].
- [26] S. Catani et al. “Top-quark pair production at the LHC: Fully differential QCD predictions at NNLO”. In: *JHEP* 07 (2019), p. 100. arXiv: 1906.06535 [hep-ph].
- [27] K. Hagiwara, Y. Sumino, and H. Yokoya. “Bound-state Effects on Top Quark Production at Hadron Colliders”. In: *Phys. Lett. B* 666 (2008), pp. 71–76. arXiv: 0804.1014 [hep-ph].
- [28] Y. Kiyo et al. “Top-quark pair production near threshold at LHC”. In: *Eur. Phys. J. C* 60 (2009), pp. 375–386. arXiv: 0812.0919 [hep-ph].
- [29] W.-L. Ju et al. “Top quark pair production near threshold: single/double distributions and mass determination”. In: *JHEP* 06 (2020), p. 158. arXiv: 2004.03088 [hep-ph].
- [30] “A precise interpretation for the top quark mass parameter in ATLAS Monte Carlo simulation”. In: *ATL-PHYS-PUB-2021-034* (2021). URL: <https://cds.cern.ch/record/2777332/>.

- [31] P. Marquard et al. “Quark Mass Relations to Four-Loop Order in Perturbative QCD”. In: *Phys. Rev. Lett.* 114.14 (2015), p. 142002. arXiv: 1502.01030 [hep-ph].
- [32] N. Gray et al. “Three-loop relation of quark \overline{MS} and pole masses”. In: *Zeitschrift für Physik C Particles and Fields* 48 (1990), pp. 673–679.
- [33] K. G. Chetyrkin and M. Steinhauser. “The Relation between the \overline{MS} and the on-shell quark mass at order α_s^3 ”. In: *Nucl. Phys. B* 573 (2000), pp. 617–651. arXiv: hep-ph/9911434.
- [34] K. Melnikov and T. v. Ritbergen. “The Three loop relation between the \overline{MS} -bar and the pole quark masses”. In: *Phys. Lett. B* 482 (2000), pp. 99–108. arXiv: hep-ph/9912391.
- [35] P. A. Baikov, K. G. Chetyrkin, and J. H. Kühn. “Quark Mass and Field Anomalous Dimensions to $\mathcal{O}(\alpha_s^5)$ ”. In: *JHEP* 10 (2014), p. 076. arXiv: 1402.6611 [hep-ph].
- [36] T. Luthe et al. “Five-loop quark mass and field anomalous dimensions for a general gauge group”. In: *JHEP* 01 (2017), p. 081. arXiv: 1612.05512 [hep-ph].
- [37] K. G. Chetyrkin, J. H. Kühn, and M. Steinhauser. “RunDec: A Mathematica package for running and decoupling of the strong coupling and quark masses”. In: *Comput. Phys. Commun.* 133 (2000), pp. 43–65. arXiv: hep-ph/0004189.
- [38] R. Tarrach. “The Pole Mass in Perturbative QCD”. In: *Nucl. Phys. B* 183 (1981), pp. 384–396.
- [39] O. V. Tarasov. “Anomalous dimensions of quark masses in the three-loop approximation”. In: *Phys. Part. Nucl. Lett.* 17.2 (2020), pp. 109–115. arXiv: 1910.12231 [hep-ph].
- [40] S. A. Larin. “The Renormalization of the axial anomaly in dimensional regularization”. In: *Phys. Lett. B* 303 (1993), pp. 113–118. arXiv: hep-ph/9302240.
- [41] K. G. Chetyrkin. “Quark mass anomalous dimension to $\mathcal{O}(\alpha_s^4)$ ”. In: *Phys. Lett. B* 404 (1997), pp. 161–165. arXiv: hep-ph/9703278.
- [42] J. A. M. Vermaseren, S. A. Larin, and T. van Ritbergen. “The four loop quark mass anomalous dimension and the invariant quark mass”. In: *Phys. Lett. B* 405 (1997), pp. 327–333. arXiv: hep-ph/9703284.
- [43] S. Dittmaier and H. Rzehak. “Electroweak renormalization based on gauge-invariant vacuum expectation values of non-linear Higgs representations. Part I. Standard Model”. In: *JHEP* 05 (2022), p. 125. arXiv: 2203.07236 [hep-ph].
- [44] A. L. Kataev and V. S. Molokoedov. “Notes on Interplay between the QCD and EW Perturbative Corrections to the Pole-Running-to-Top-Quark Mass Ratio”. In: *JETP Lett.* 115.12 (2022), pp. 704–712. arXiv: 2201.12073 [hep-ph].
- [45] A. H. Hoang, C. Lepenik, and M. Preisser. “On the Light Massive Flavor Dependence of the Large Order Asymptotic Behavior and the Ambiguity of the Pole Mass”. In: *JHEP* 09 (2017), p. 099. arXiv: 1706.08526 [hep-ph].
- [46] A. H. Hoang, C. Lepenik, and V. Mateu. “REvolver: Automated running and matching of couplings and masses in QCD”. In: *Comput. Phys. Commun.* 270 (2022), p. 108145. arXiv: 2102.01085 [hep-ph].
- [47] K. G. Chetyrkin, J. H. Kuhn, and C. Sturm. “QCD decoupling at four loops”. In: *Nucl. Phys. B* 744 (2006), pp. 121–135. arXiv: hep-ph/0512060.
- [48] Y. Schroder and M. Steinhauser. “Four-loop decoupling relations for the strong coupling”. In: *JHEP* 01 (2006), p. 051. arXiv: hep-ph/0512058.

- [49] J. H. Kühn, A. Scharf, and P. Uwer. “Electroweak effects in top-quark pair production at hadron colliders”. In: *Eur. Phys. J. C* 51 (2007), pp. 37–53. arXiv: hep-ph/0610335.
- [50] M. Czakon et al. “Top-pair production at the LHC through NNLO QCD and NLO EW”. In: *JHEP* 10 (2017), p. 186. arXiv: 1705.04105 [hep-ph].
- [51] S. Catani et al. “Top-quark pair hadroproduction at NNLO: differential predictions with the \overline{MS} mass”. In: *JHEP* 08.08 (2020), p. 027. arXiv: 2005.00557 [hep-ph].
- [52] A. H. Hoang and T. Teubner. “Top quark pair production close to threshold: Top mass, width and momentum distribution”. In: *Phys. Rev. D* 60 (1999), p. 114027. arXiv: hep-ph/9904468.
- [53] A. H. Hoang, C. J. Reisser, and P. Ruiz-Femenia. “Phase Space Matching and Finite Lifetime Effects for Top-Pair Production Close to Threshold”. In: *Phys. Rev. D* 82 (2010), p. 014005. arXiv: 1002.3223 [hep-ph].
- [54] M. Beneke et al. “Non-resonant and electroweak NNLO correction to the e^+e^- top anti-top threshold”. In: *JHEP* 02 (2018), p. 125. arXiv: 1711.10429 [hep-ph].
- [55] F. Bach et al. “Fully-differential Top-Pair Production at a Lepton Collider: From Threshold to Continuum”. In: *JHEP* 03 (2018), p. 184. arXiv: 1712.02220 [hep-ph].
- [56] S. Alekhin, J. Blümlein, and S. Moch. “NLO PDFs from the ABMP16 fit”. In: *Eur. Phys. J. C* 78.6 (2018), p. 477. arXiv: 1803.07537 [hep-ph].
- [57] S. Alekhin et al. “Parton distribution functions, α_s , and heavy-quark masses for LHC Run II”. In: *Phys. Rev. D* 96 (2017), p. 014011. arXiv: 1701.05838 [hep-ph].
- [58] T. Mäkelä. “Towards global interpretation of LHC data: SM and EFT couplings from jet and top quark measurements at CMS”. Dissertation, Universität Hamburg. PhD thesis. 2022, 213 pages: Illustrations, figures. URL: <https://bib-pubdb1.desy.de/record/482499>.
- [59] A. M. Sirunyan et al. “Measurement of the $t\bar{t}$ production cross section, the top quark mass, and the strong coupling constant using dilepton events in pp collisions at $\sqrt{s} = 13$ TeV”. In: *Eur. Phys. J. C* 79.5 (2019), p. 368. arXiv: 1812.10505 [hep-ex].
- [60] M. M. Defranichis et al. “Running of the top quark mass at NNLO in QCD”. In: (Aug. 2022). arXiv: 2208.11399 [hep-ph].
- [61] M. Butenschön et al. “Top Quark Mass Calibration for Monte Carlo Event Generators”. In: *Phys. Rev. Lett.* 117.23 (2016), p. 232001. arXiv: 1608.01318 [hep-ph].